Appendix 6.0

31/07/13

(1)

Antiparticles: proof of concept of the quantal vacuum and of medium polarization effects

Let us consider a massive quantal particle, e.g. an electron, which moves at a velocity close to that of light. Because of Heisenberg's relations, there exists a finite probability to observe the particle moving with a velocity larger than its average velocity, and thus faster than light, a possibility ruled out by special relativity. The only way to avoid this, is by introducing antiparticles, that is, a hole in a "vacuum", filled to the rim (Fermi energy) with particles, thus providing the physics to the negative energy solutions of Dirac's equation.

In other words, when an electron approaches the maximum speed with which information propagates in a medium, like e.g., in the case of the electron, the QED vacuum, processes like the one depicted in Fig. 1 become operative

6.C.1

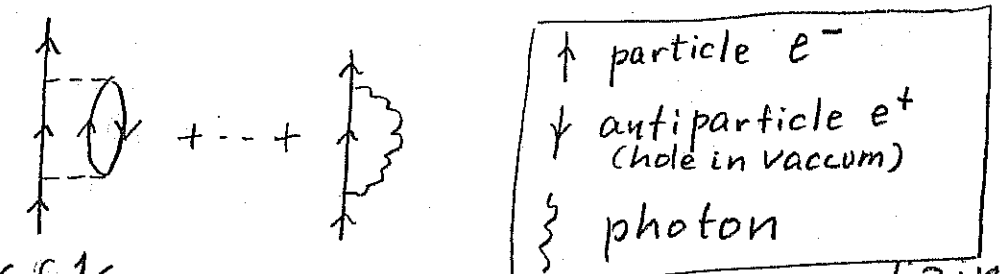

6.C.1

Fig. 1 Feynman diagrams renormalizing the properties of an electron

In other words, one can take care of the position indeterminacy of a quantal particle (electron) accepting the possibility to observe it through specific measurements which unavoidably create different particles, each of of them identical to the original one, but with different positions. To keep track of conserved quantum numbers, these particles are to be accompanied by an equal number of antiparticles (positrons).

Similar results can be obtained by considering vacuum fluctuations, (ZPF), and forcing them to become real through e.g. the Pauli principle, as observed in the Lamb shift (Fig. 6.C.2; cf. also App. D)

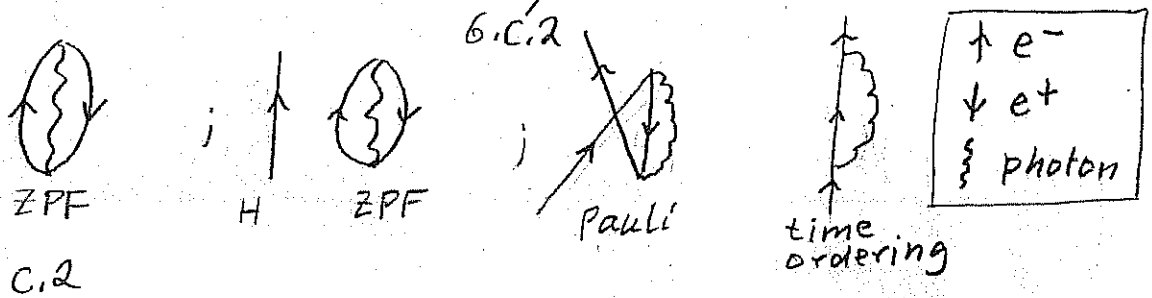

6.C.2

Fig. 6.C.2: QED vacuum fluctuation (ZPF). In presence of e.g. an hydrogen atom (H), its electron is forced by Pauli principle to exchange with that of the ZPF, leading to a CO (correlation-like) process. Time ordering leads to PO (polarization) processes.

In the nuclear case the medium can, due to spatial quantization typical of Finite Many-Body Systems (FMBS), propagate information with varied frequency. Typically,

few MeV (low-lying collective vibrations) (3) and tens of MeV (giant resonances), leading to a rich number of CO and PO processes. This is in keeping with the fact that the intermediate boson (photon QED, vibrations of nuclear medium) propagates in a medium which is not isotropic, thus undergoing fragmentation of the associated strength (inhomogeneous damping). To make even richer the nuclear scenario, collisional 6.C.3 damping plays also a role in the strength function of GR. Nonetheless, the associated widths (lifetimes) are controlled by the coupling to doorway states, even at nuclear temperatures of 1-2 MeV (Fig. 3). The strong cancellation found between self-energy and vertex correction diagrams, testify to the collectivity of nuclear vibrations, and reminds Furry's theorem (no coupling between one- and two-photon states),

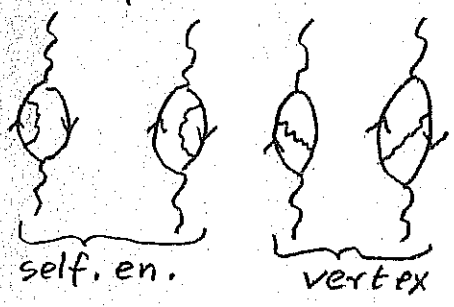

Fig. 3 6.C.3
Lowest order diagrams which dress collective nuclear vibrations and GR.

Summing up, nothing is really free in the quantal world. Selected measurements carried out with specific probes, can make virtual processes become real, and shed light on the variety of these processes leading to effective fields (dressed fermions and bosons),

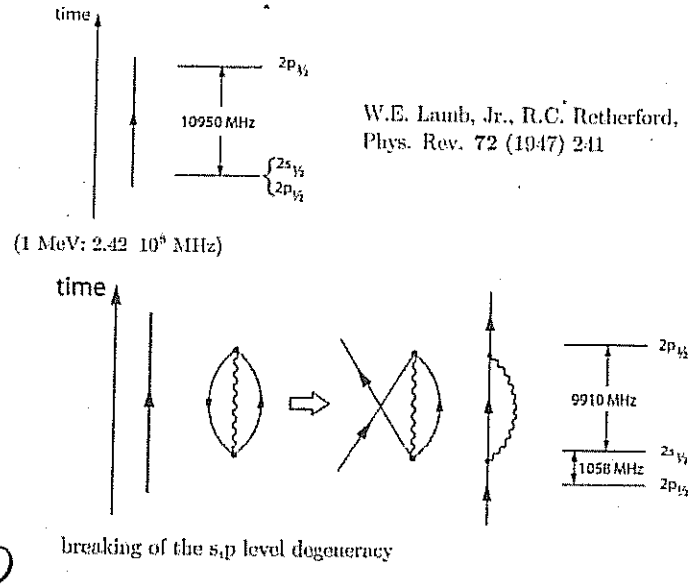

Figure 6.C.1: Schematic representation of the processes associated with the Lamb shift.

are given. The sum of contributions (a) and (b) can, in principle, be represented by a renormalized vertex (cf. digram (c)). It is of notice, however, that there is, as a rule, conspicuous interference (e.g. cancellation) in the nuclear case between vertex and self–energy contributions (cf. diagrams (a) and (d)+(e) of Fig. 6.D.2, a phenomenon closely related with conservation laws (generalized Ward identities)). In particular, cancellation in the case in which the bosonic modes are isoscalar. Consequently, one has to sum explicitly the different amplitudes with the corresponding phases and eventually take the modulus squared of the result to obtain the quantities to be compared with the data, a fact that precludes the use of an effective, ω–independent (renormalized) vertex.

Within the framework of QED the above mentioned cancellations are exact implying that the interaction between one– and two–photon states vanishes (Furry theorem). The physics at the basis of the cancellation found in the nuclear case can be exemplified by looking at a spherical nucleus displaying a low–lying collective quadrupole vibration. The associated zero point fluctuations (ZPF) lead to time dependent shapes with varied instantaneous values of the quadrupole moment, and of its orientation (dynamical spontaneous breaking of rotational invariance). In other words, a component of the ground state wavefunction ($|(j_p \otimes j_h^{-1})_{2^+} \otimes 2^+; 0^+\rangle$), which can be viewed as a gas of quadrupole (quasi) bosons promoting a nucleon across the Fermi energy (particle–hole excitation) will lead to fermionic states which behave as having a positive (particle) and a negative (hole) effective quadrupole moment, in keeping with the fact that the closed shell system is spherical, thus carrying zero quadrupole moment.

Appendix 6.E Single–nucleon transfer for pedestrians

In this Appendix we discuss some aspects of the relations existing between nuclear structure and one–particle transfer cross sections. To do so, we repeat some of the

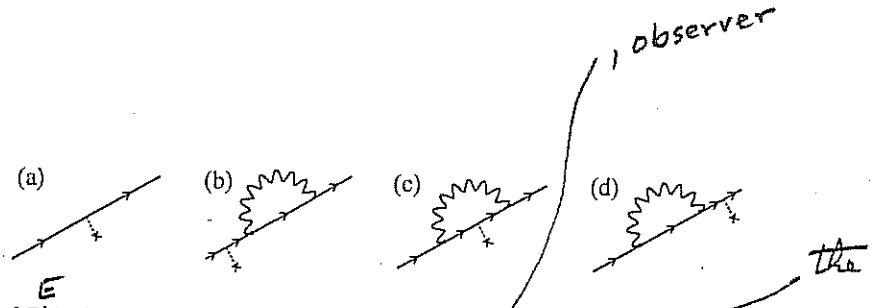

Figure 6.1: Self energy (effective–mass–like) processes. The result of the probing with an external field (dotted line started with a cross) of the properties (mass, single–particle energy, etc) of a fermion (e.g. an electron or a nucleon, arrowed line) dressed through the coupling of (quasi) bosons (photons or collective vibrations, wavy line), corresponds to the modulus squared of the sum of the amplitudes associated with each of the four diagrams (a)–(d) (cf. (Feynman, 1975)).

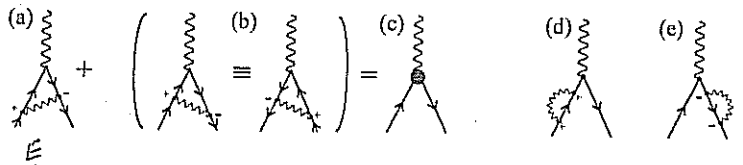

Figure 6.2: Vertex corrections. These are triple–interaction vertex diagrams in which none of the incoming lines can be detached from either of the other two by cutting one line. Migdal's (1958) theorem states that, for phonons and electrons (Bardeen–Pines mechanism to break gauge invariance), vertex corrections can be neglected, but usually they are not negligible, in any case not in nuclei (cancellation) (cf. e.g. Anderson (1984)). The solid circle in (c) represents the effective, renormalized vertex.

steps carried out in the text but this time in a simpler and straightforward way, ignoring the complications associated with the spin carried out by the particles, the spin–orbit dependence of the optical model potential, the recoil effect, etc.

We consider the case of $A(d, p)A + 1$ reaction, namely that of neutron stripping. The intrinsic wave functions ψ_α and ψ_β, where $\alpha = (A, d)$ and $\beta = ((A + 1), p)$,

$$\psi_\alpha = \psi^{I_A}_{M_A}(\xi_A)\phi_d(\vec{r}_{np}), \tag{6.E.1a}$$

$$\psi_\beta = \psi^{I_{A+1}}_{M_{A+1}}(\xi_{A+1}) = \sum_{l,I'_A}(I'_A; l]\}I_{A+1})[\psi^{I'_A}(\xi_A)\phi^l(\vec{r}_n)]^{I_{A+1}}_{M_{A+1}-M_A}, \tag{6.E.1b}$$

where $(I'_A; l]\}I_{A+1})$ is a generalized fractional parentage coefficient. It is of notice that this fractional parentage expansion is not well defined. In fact, as a rule, $(I'_A; l]\}I_{A+1})\phi^l(\vec{r}_n)_{M_{A+1}-M_A}$ is an involved, dressed quasiparticle state containing only a fraction of the "pure" single particle strength (cf. Apps 6.A and 6.B). For simplicity we assume the expansion is operative. To further simplify the derivation we assume we are dealing with spinless particles. The variable $\vec{r}_{np}$ is the relative coordinate of the proton and the neutron (see Fig. 6.E.1).

The transition matrix element can now be written as

$$\begin{aligned} T_{d,p} &= \langle\psi^{I_{A+1}}_{M_{A+1}}(\xi_{A+1})\chi^{(-)}_p(k_p, \vec{r}_p), V'_\beta\psi^{I_A}_{M_A}(\xi_A)\chi^{(+)}_d(k_d, \vec{r}_d)\rangle \\ &= \sum_{\substack{l,I'_A \\ M'_A}}(I'_A; l]\}I_{A+1})(I'_A\, M'_A\, l\, M_{A+1} - M'_A|I_{A+1}\, M_{A+1}) \\ &\times \int d\vec{r}_n d\vec{r}_p \chi^{*(-)}_p(k_p, \vec{r}_p)\phi^{*l}_{M_{A+1}-M'_A}(\vec{r}_n)(\psi^{I_A}_{M_A}(\xi_A), V'_\beta\psi^{I'_A}_{M'_A}(\xi_A)) \\ &\times \phi_d(\vec{r}_{np})\chi^{(+)}_d(k_d, \vec{r}_d)\,\delta_{I'_A,I_A}\,\delta_{M'_A,M_A}. \end{aligned} \tag{6.E.2}$$

In the stripping approximation

$$\begin{aligned} V'_\beta &= V_\beta(\xi, \vec{r}_\beta) - \bar{U}_\beta(r_\beta) \\ &= V_\beta(\xi_A, \vec{r}_{pA}) + V_\beta(\vec{r}_{pn}) - \bar{U}_\beta(r_{pA}). \end{aligned} \tag{6.E.3}$$

Then

$$\begin{aligned} (\psi^{I_A}_{M_A}(\xi_A), V'_\beta\psi^{I_A}_{M_A}(\xi_A)) &= (\psi^{I_A}_{M_A}(\xi_A), V_\beta(\xi_A, \vec{r}_{pA})\psi^{I_A}_{M_A}(\xi_A)) \\ &+ (\psi^{I_A}_{M_A}(\xi_A), V_\beta(\vec{r}_{pn})\psi^{I_A}_{M_A}(\xi_A)) - \bar{U}_\beta(r_{pA}). \end{aligned} \tag{6.E.4}$$

We assume

$$U_\beta(r_{pA}) = (\psi^{I_A}_{M_A}(\xi_A), V_\beta(\xi_A, \vec{r}_{pA})\psi^{I_A}_{M_A}(\xi_A)). \tag{6.E.5}$$

Then

$$(\psi^{I_A}_{M_A}(\xi_A), V'_\beta\psi^{I_A}_{M_A}(\xi_A)) = V_{np}(\vec{r}_{pn}). \tag{6.E.6}$$

Inserting eq. (6.E.6) into eq. (6.E.2) we obtain

$$\begin{aligned} T_{d,p} &= \sum_l (I_A; l]\}I_{A+1})(I_A\, M_A\, l\, M_{A+1} - M_A|I_{A+1}\, M_{A+1}) \\ &\times \int d\vec{r}_n d\vec{r}_p \chi^{*(-)}_p(k_p, \vec{r}_p)\phi^{*l}_{M_{A+1}-M_A}(\vec{r}_n)V(\vec{r}_{pn})\phi_d(\vec{r}_{np})\chi^{(+)}_d(k_d, \vec{r}_d) \end{aligned} \tag{6.E.7}$$

This is the reason why no "intrinsic" proton wavefunction appears in (6.F.16)

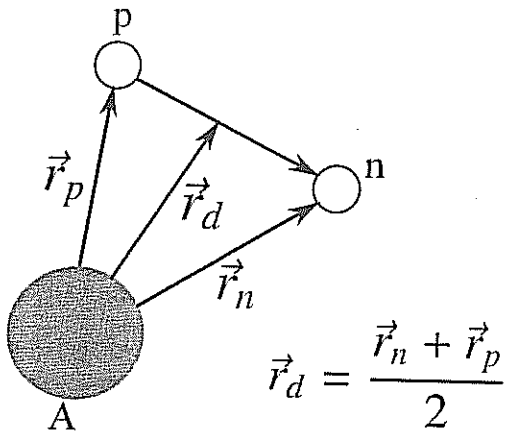

Figure 6.E.1: Coordinates used in the description of the $A(d, p)(A+1)$ stripping process.

The differential cross section is then equal to

$$\frac{d\sigma}{d\Omega} = \frac{2}{3}\frac{\mu_p\mu_d}{(2\pi\hbar^2)^2}\frac{(2I_{A+1}+1)}{(2I_A+1)}\frac{k_p}{k_d}\sum_{l,m_l}\frac{(I_A; l]I_{A+1})^2}{2l+1}|B^l_{m_l}|^2, \qquad (6.E.8)$$

where

$$B^l_{m_l}(\theta) = \int d\vec{r}_n d\vec{r}_p \chi^{*(-)}_p(k_p, \vec{r}_p) Y^{*l}_m(\hat{r}_n) u_{nl}(r_n) V(\vec{r}_{pn}) \phi_d(\vec{r}_{np}) \chi^{(+)}_d(k_d, \vec{r}_d) \qquad (6.E.9)$$

and

$$\phi^l_m(\vec{r}_n) = u_{nl}(r_n) Y^l_m(\hat{r}_n), \qquad (6.E.10)$$

is the single-particle wave function of a neutron ~~moving in~~ the core A. For simplicity, the radial wave function $u_{nl}(r_n)$ can be assumed to be a solution of a Saxon-Woods potential of parameters $V_0 \approx 50$ MeV, $a = 0.65$ fm and $r_0 = 1.25$ fm.

The relation (6.E.8) gives the cross section for the ~~stripping~~ from the projectile of a neutron that would correspond to the n^{th} valence neutron in the nucleus $(A+1)$. If we now want the cross section for stripping any of the valence nutrons of the final nucleus from the projectile, we must multiply eq. (6.E.8) by n. A more careful treatment of the antisymmetry with respect to the neutrons ~~shoes~~ this to be the correct answer.

Finally we get

$$\frac{d\sigma}{d\Omega} = \frac{(2I_{A+1}+1)}{(2I_A+1)}\sum_l S_l \sigma_l(\theta), \qquad (6.E.11)$$

where

$$S_l = n(I_A; l]I_{A+1})^2, \qquad (6.E.12)$$

and

$$\sigma_l(\theta) = \frac{2}{3}\frac{\mu_p\mu_d}{(2\pi\hbar^2)^2}\frac{k_p}{k_d}\frac{1}{2l+1}\sum_m |B^l_m|^2 \qquad (6.E.13)$$

The distorted wave programs numerically evaluate the quantity $B^l_{m_l}(\theta)$, using for the wave functions $\chi^{(-)}$ and $\chi^{(+)}$ the solution of the optical potentials that fit the elastic scattering, i.e.

$$(-\nabla^2 + \bar{U} - k^2)\chi = 0, \qquad (6.E.14)$$

(see ~~eq. (6.E.15)~~). Note that if the target nucleus is even, $I_A = 0$, $l = I_{A+1}$. That is, only one l value contributes in eq. (6.E.8), and the angular distribution is uniquely given by $\sum_m |B^l_m|^2$. The l-dependence of the angular distributions helps to identify $l = I_{A+1}$. The factor S_l needed to normalize the calculated function to the data yields (assuming a good fit to the angular distribution), is known in the literature as the spectroscopic factor. It was assumed not only that it could be defined, but also that it contained all the nuclear structure information (aside from that associated with the angular distribution) which could be extracted from single–particle transfer. In other words, that it was the bridge directly connecting theory with experiment. Because nucleons are never bare, but are dressed by the coupling to collective modes ~~(cf. App. 6.A)~~, the spectroscopic factor approximation is at best a helpful tool to get order of magnitude information from one–particle transfer data.

There is a fundamental problem which makes the handling of integrals like that of (6.E.9) difficult to handle, if not numerically at least conceptually. This difficulty is connected with the so called recoil effect [2], namely the fact that the center of mass of the two interacting particles in entrance ($\mathbf{r}_\alpha : \alpha = a + A$) and exit ($\mathbf{r}_\beta : \beta = b + B$) channels is different. This is at variance with what one is accustomed to deal with in nuclear structure calculations, in which the Hartree potential depends on a single coordinate, as well as in the case of elastic and inelastic reactions, situations in which $\mathbf{r}_\alpha = \mathbf{r}_\beta$. When $\mathbf{r}_\alpha \neq \mathbf{r}_\beta$ we enter a rather more complex many–body problem, in particular if continuum states are to be considered, than nuclear structure practitioners were accustomed to.

Of notice that similar difficulties have been faced in connection with the non–local Fock (exchange) potential. As a rule, the corresponding (HF) mean field equations are rendered local making use of the k–mass approximation or within the framework of Local Density Functional Theory (DFT), in particular with the help of the Kohn–Sham equations (see e.g. C. Mahaux et al. (1985), Broglia, ~~et al.~~ (2004) and refs. therein). Although much of the work in this field is connected with the correlation potential (interweaving of single–particle and collective motion), an important fraction is connected with the exchange potential.

In any case, and returning to the subject of the present appendix, it is always useful to be able to introduce approximations which can help the physics which is at the basis of the phenomenon under discussion (single–particle motion) emerge in a natural way, if not to compare in detail with the experimental data. Within this context, to reduce the integral (6.E.9) one can assume that the proton-neutron interaction V_{np} has zero-range, i.e.

$$V_{np}(\vec{r}_{np})\phi_d(\vec{r}_{np}) = D_0\delta(\vec{r}_{np}) \qquad (6.E.15)$$

so that B^l_m becomes equal to

$$B^l_{m_l}(\theta) = D_0 \int d\vec{r}\chi^{*(-)}_p(k_p,\vec{r})Y^{*l}_{m_l}(\hat{r})u_l(r)\chi^{(+)}_d(k_d,\vec{r}), \qquad (6.E.16)$$

which is a three dimensional integral, but in fact essentially a one–dimensional integral, as the integration over the angles ~~is simple to carry out.~~ can be worked out analitically.

[2] While this effect could be treated in a cavalier fashion in the case of light ion reactions ($m_a/m_A \ll 1$), this was not possible in the case of heavy ion reactions, as the change in momenta involved was always sizeable (cf. Broglia and Winther (2004) and refs. therein).

6.E.1 Plane-wave limit

If in Eq. (6.E.14) one sets $\bar{U} = 0$, the distorted waves become plane waves i.e.

$$\chi_d^{(+)}(k_d, \vec{r}) = e^{i\vec{k}_d\cdot\vec{r}}, \tag{6.E.17a}$$

$$\chi_d^{*(-)}(k_p, \vec{r}) = e^{-i\vec{k}_p\cdot\vec{r}}. \tag{6.E.17b}$$

Equation (6.E.16) can now be written as

$$B_m^l = D_0 \int d\vec{r} e^{i(\vec{k}_d - \vec{k}_p)\cdot\vec{r}} Y_m^{*l}(\hat{r}) u_l(r). \tag{6.E.18}$$

The linear momentum transferred to the nucleus is $\vec{k}_d - \vec{k}_p = \vec{q}$. Let us expand $e^{i\vec{q}\cdot\vec{r}}$ in spherical harmonics, i.e.

$$\begin{aligned} e^{i\vec{q}\cdot\vec{r}} &= \sum_l i^l j_l(qr)(2l+1)P_l(\hat{q}\cdot\hat{r}) \\ &= 4\pi \sum_l i^l j_l(qr) \sum_m Y_m^{*l}(\hat{q}) Y_m^l(\hat{r}), \end{aligned} \tag{6.E.19}$$

so

$$\int d\hat{r} e^{i\vec{q}\cdot\vec{r}} Y_m^l(\hat{r}) = 4\pi i^l j_l(qr) Y_m^{*l}(\hat{q}). \tag{6.E.20}$$

Then

$$\begin{aligned} \sum_m |B_m^l|^2 = \sum_m |Y_m^l(\hat{q})|^2 D_0^2 16\pi^2 \times \\ \left| \int r^2 dr j_l(qr) u_l(r) \right|^2 = \\ \frac{2l+1}{4\pi} D_0^2 16\pi^2 \left| \int r^2 dr j_l(qr) u_l(r) \right|^2. \end{aligned} \tag{6.E.21}$$

Thus, the angular distribution is given by the integral $\left|\int r^2 dr j_l(qr) u_l(r)\right|^2$. If one assumes that the process takes place mostly on the surface, the angular distribution will be given by $|j_l(qR_0)|^2$, where R_0 is the nuclear radius.

We then have

$$\begin{aligned} q^2 &= k_d^2 + k_p^2 - 2k_d k_p \cos(\theta) \\ &= (k_d^2 + k_p^2 - 2k_d k_p) + 2k_d k_p (1 - \cos(\theta)) \\ &= (k_d - k_p)^2 + 4k_d k_p \, (\sin(\theta/2))^2 \\ &\approx 4k_d k_p \, (\sin(\theta/2))^2, \end{aligned} \tag{6.E.22}$$

since $k_d \approx k_p$ for stripping reactions at typical energies. Thus the angular distribution has a diffraction-like structure given by

$$|j_l(qR_0)|^2 = j_l^2(2R_0\sqrt{k_d k_p}\sin(\theta/2)). \tag{6.E.23}$$

The function $j_l(x)$ has its first maximum at $x = l$, i.e. where

$$\sin(\theta/2) = \frac{l}{2R_0 k}, \qquad (k_p \approx k_d = k), \tag{6.E.24}$$

Examples of the above relation are provided in Fig. 6.E.2

Fig 6.E.2

Plane-wave approximation analysis of three $^{44}Ca(d,p)^{45}Ca$ differential cross sections leading to the ground state ($\ell=3$) and to the 1.9 MeV ($\ell=1$) and 2.4 MeV ($\ell=0$) excited states, i.e. $f_{7/2}$, $p_{1/2}$ and $s_{1/2}$ states (Cobb and Guthe, 1957)

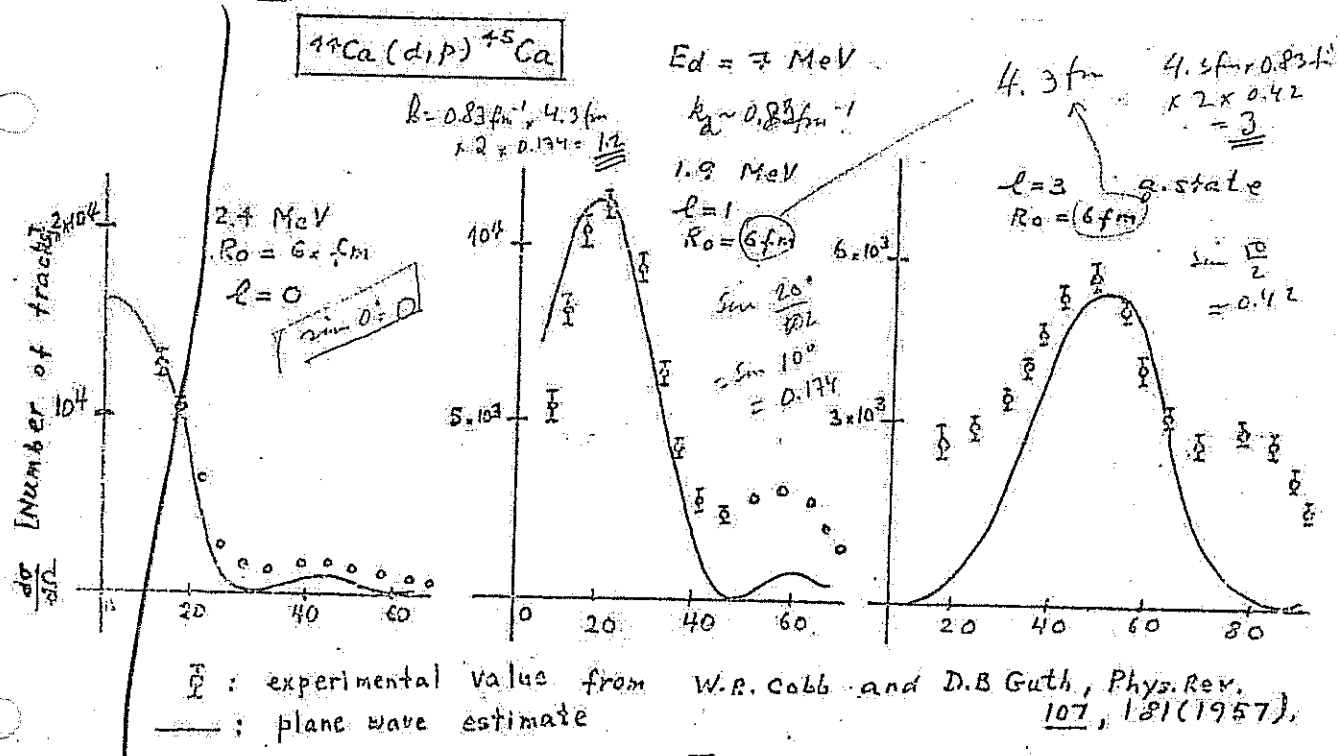

F : experimental value from W.R. Cobb and D.B Guth, Phys. Rev. 107, 181 (1957).
—— : plane wave estimate

Figure 6.E.2:

Gregory
Hay la figura
correcta con los
datos experimentales

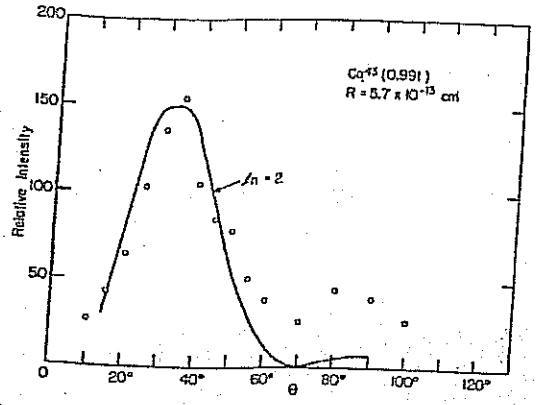

FIG. 7. Angular distribution of proton group corresponding to Ca^{43} level at 0.991 Mev, with stripping curve calculated for $l_n=2$, $R=5.7\times10^{-13}$ cm.

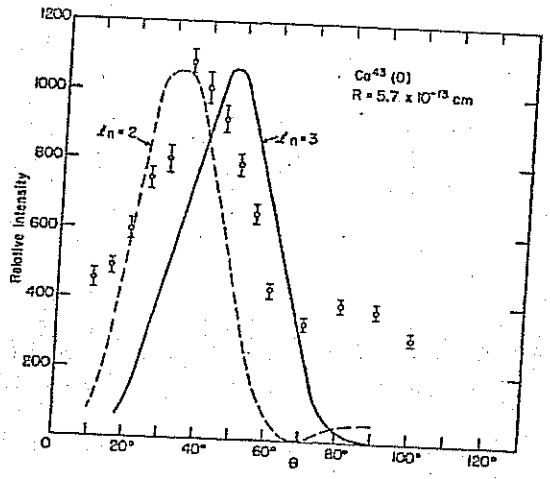

FIG. 8. Angular distribution of proton group associated with formation of the ground state of Ca^{43}, with stripping curves calculated for $l_n=2$ and 3, $R=5.7\times10^{-13}$ cm.

The relation of this work to the β-decay studies[11] has been discussed in detail by Braams.[2] A theoretical interpretation of the angular distributions and relative intensities of the odd-parity levels below 2.1-Mev excitation has been offered by French and Raz.[16] The results of this and other experiments are shown to be consistent with a shell-model picture. Strict j-j coupling predicts

$$\sigma(Ca^{43}\text{ ground state}):\sigma(Ca^{41}\text{ ground state})=0.75,$$

compared to 0.69 observed. That even-parity states exist as low as 1 Mev emphasizes the fact that the Ca^{42} core is rather easily disarranged. One of the five $l_n=1$ levels above 2.6-Mev is probably the "single-particle" $p_{\frac{1}{2}}$ state, that is, $[(f_{7/2})^2]_{J=0}p_{\frac{1}{2}}$, split by 0.5 to 1.5 Mev from the $[(f_{7/2})^2]_{J=0}p_{\frac{3}{2}}$ level at 2.05 Mev. No evidence is found for a $[(f_{7/2})^2]_{J=0}f_{\frac{1}{2}}$ level.

To Wilton Tripp, Sylvia Darrow, Janet Rose, and Estelle Freedman, we wish to express our gratitude for their patient and accurate plate counting. Thanks are also due to Lt. Douglas B. Guthe, USN, and to Salvatore Buccino for their help in the computations.

[16] J. B. French and B. J. Raz, Phys. Rev. 104, 1411 (1956).

PHYSICAL REVIEW VOLUME 107, NUMBER 1 JULY 1, 1957

Angular Distribution of Protons from the $Ca^{44}(d,p)Ca^{45}$ Reaction*†

W. R. COBBE‡ AND D. B. GUTHE‡
Physics Department and Laboratory for Nuclear Science, Massachusetts Institute of Technology, Cambridge, Massachusetts
(Received March 26, 1957)

The broad-range magnetic spectrograph has been used to study proton groups produced from thin Ca^{44} targets bombarded by 7-Mev deuterons. The angular distributions and relative intensities of groups corresponding to levels in Ca^{45} were measured. Stripping theory was employed to determine the angular momenta of the captured neutrons.

I. INTRODUCTION

THE present work reports one of a series of experiments on the calcium isotopes undertaken at this laboratory over the past three years. The work of Braams[1] is here extended to obtain angular distributions of the proton groups associated with the previously observed levels in Ca^{45} in the range from 0 to 3.5-Mev excitation.

Ca^{45} decays by β^- emission to stable Sc^{45}. The values[2] of spin $\frac{7}{2}$ and magnetic moment 4.75 nuclear magnetons[3]

* This work has been supported in part by the joint program of the Office of Naval Research and the U. S. Atomic Energy Commission.

† Much of the work reported here is from a joint thesis submitted by the authors to Massachusetts Institute of Technology in partial fulfillment of the requirements for the degree of Master of Science in Physics under the Naval Postgraduate Training Program.

‡ Lieutenant, U. S. Navy.

[1] C. M. Braams, Ph.D. thesis, University of Utrecht, Utrecht, Netherlands, July, 1956 (unpublished).
[2] H. Schuler and T. Schmidt, Naturwissenschaften 22, 758 (1934); and H. Kopfermann and E. Rasmussen, Z. Physik 92, 82 (1934).
[3] W. G. Proctor and F. C. Yu, Phys. Rev. 81, 20 (1951).

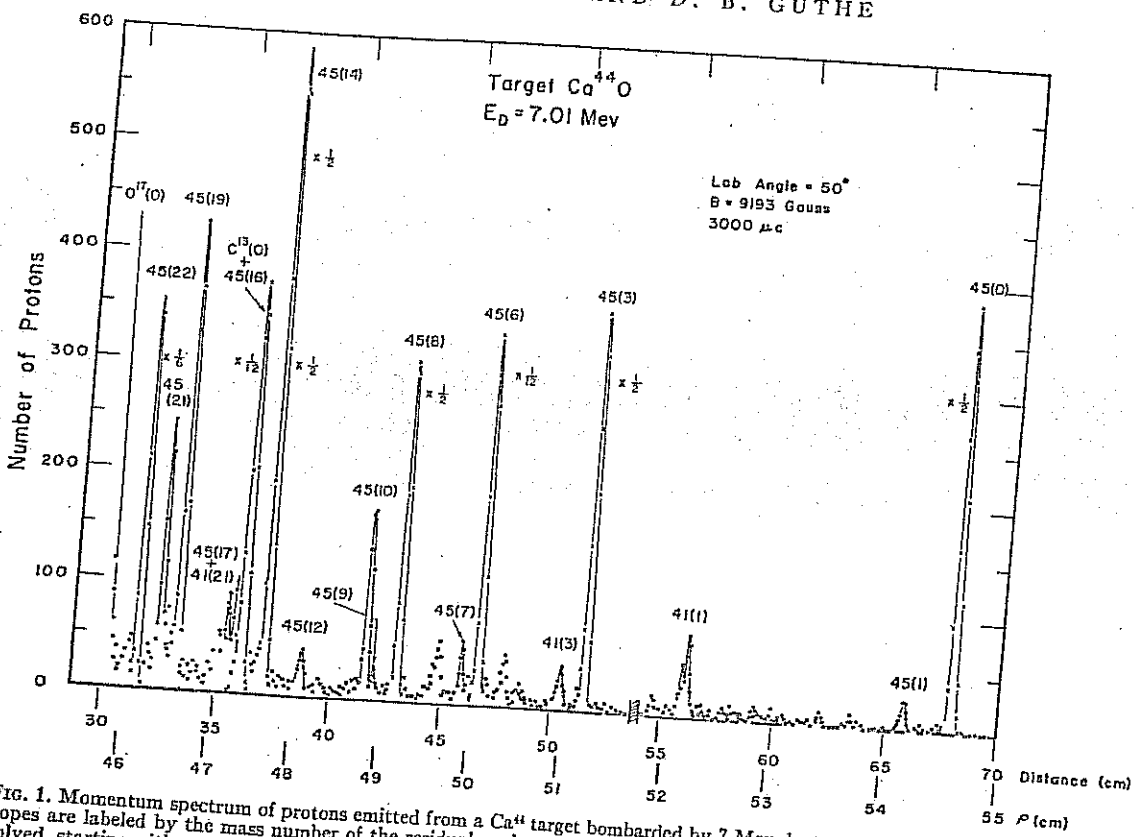

FIG. 1. Momentum spectrum of protons emitted from a Ca^{44} target bombarded by 7-Mev deuterons. The peaks assigned to calcium isotopes are labeled by the mass number of the residual nucleus, followed in parentheses by a number denoting the particular state involved, starting with zero for the ground state; the number is that assigned in reference 1.

measured for Sc^{45} indicate a ground state in agreement with the shell-model prediction of an $f_{7/2}$ orbit for the odd proton. The beta decay has a half-life of 163.5 days[4] and an allowed shape.[5] This leads to $\log ft=5.9$. If the beta decay is presumed to be allowed, it is consistent with the prediction that the ground state of Ca^{45} is characterized by an f orbit for the odd neutron. Since $I=0$ for the ground state of Ca^{44}, the angular distribution of protons forming the ground state of Ca^{45} in the (d,p) reaction is expected to display the stripping shape characteristic of the capture of a neutron with three units of orbital angular momentum; that is, $l_n=3$.

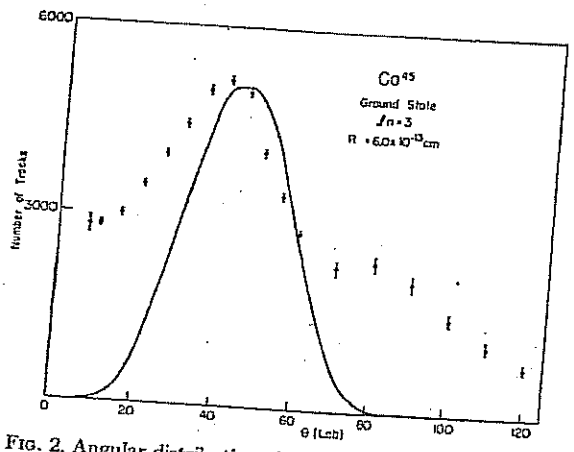

FIG. 2. Angular distribution of proton group corresponding to the ground state of Ca^{45}.

II. EXPERIMENTAL PROCEDURE

The experimental arrangements at the MIT-ONR electrostatic generator,[6] the broad-range spectrograph,[7] and the techniques adopted in using these facilities for an angular-distribution measurement[8] are described in detail in the cited references. Briefly, charged particles emerging from the bombarded target were deflected in the magnetic field of the spectrograph and then detected on Eastman NTA 25-micron photographic plates. The positions of the tracks along the plates determine the radii of curvature of the particles. Calibration of the

[4] C. F. G. Delaney and J. H. J. Poole, Phys. Rev. 89, 529 (1953).
[5] Macklin, Feldman, Lidofsky, and Wu, Phys. Rev. 77, 137 (1950).
[6] Buechner, Sperduto, Browne, and Bockelman, Phys. Rev. 91, 1502 (1953).
[7] C. P. Browne and W. W. Buechner, Rev. Sci. Instr. 27, 899 (1956).
[8] Bockelman, Braams, Browne, Buechner, Sharp, and Sperduto, Phys. Rev. 106, 176 (1957), preceding paper.

distance along the plate was made previously by comparison with the position of polonium alpha particles deflected in the instrument. The plates were read by counting the number of tracks within each half-millimeter section along the plate. To facilitate plate reading, the emulsions were covered with aluminum foil during exposure to prevent charged particles heavier than protons from reaching the plates.

The target used was prepared by Braams[1] by evaporation of CaO enriched in Ca^{44} onto a thin film of Formvar backed by gold leaf. The target material was received in the form of $CaCO_3$ from the Stable Isotopes Division, Oak Ridge, Tennessee. The calcium content was 97.99% Ca^{44}; the rest was mainly Ca^{40} of abundance 1.87%.

Normalization of the runs at each angle was accomplished by current integration. To insure that there was no change in the target that might have affected the intensities of the observed proton groups during the successive runs at the various angles, standardizing runs were periodically made at an angle of 60 degrees. The sum of the number of tracks corresponding to the ground state and to the 1.43- and 2.25-Mev levels was used for comparison. The results indicated that there was no loss of Ca^{44} from the target. An experimental check was made to insure that the several antiscattering diaphragms in the spectrograph were not collimating the beam and thereby to guarantee that the spectrograph solid angle was independent of the angle of observation.

III. RESULTS

Experimental data for the angular distribution were obtained with two bombardment exposures at each angle up to 60 degrees because of the differences in the intensities of the proton groups associated with the formation of the various levels. A 3000-microcoulomb exposure was used to secure data for the groups corresponding to the ground state and to the levels at 0.176, 1.971, 2.356, 2.394, 2.681, 2.970, and 3.319 Mev. A 500-microcoulomb exposure was used to obtain data for the groups corresponding to the levels at 1.432, 1.902, 2.249, 2.844, 3.244, and 3.419 Mev. All data acquired at angles between 70 and 120 degrees were obtained with a 500-microcoulomb exposure.

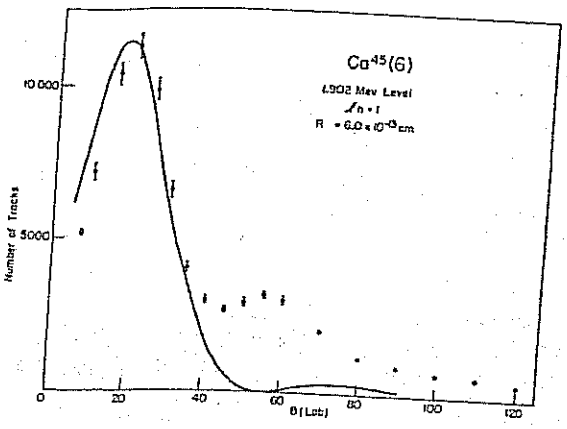

FIG. 4. Angular distribution of the proton group corresponding to the 1.902-Mev level of Ca^{45}.

Figure 1 shows representative data obtained with a 3000-microcoulomb exposure. The half-widths of the peaks observed in the experiment varied from 1.8 to 3.0 millimeters, corresponding to energy spreads of 16 to 23 kev. The peak width was caused by a combination of target thickness and slit opening. The identification of the groups, as well as the excitation energies to which they correspond, was obtained directly from the work of Braams.[1] The numbers used to label the peaks are those assigned in that work. Unlabeled weak groups, such as those in Fig. 1, at distances of 45 and 48 cm appear to arise from impurities in the target.

The angular distributions were obtained by adding at each angle the number of tracks in the appropriate peak. Figures 2 through 12 show the experimental

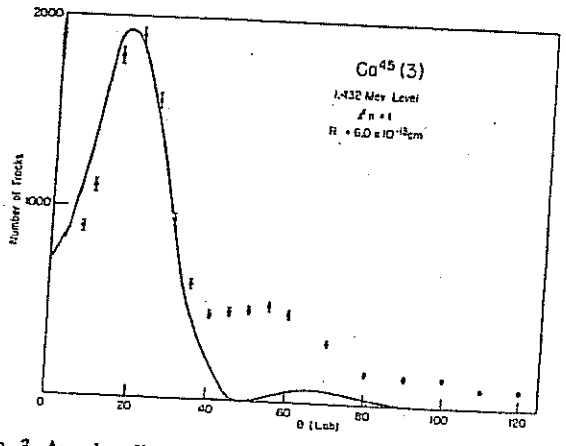

FIG. 3. Angular distribution of the proton group corresponding to the 1.432-Mev level of Ca^{45}.

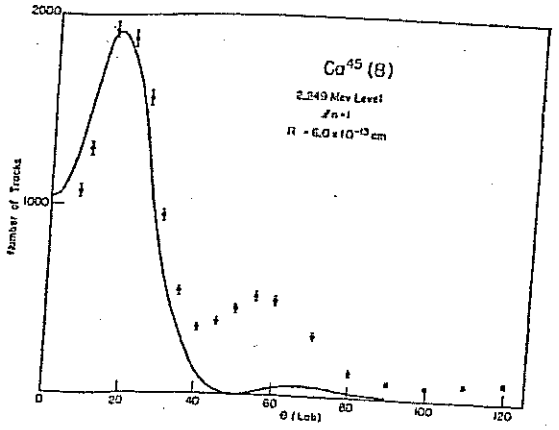

FIG. 5. Angular distribution of the proton group corresponding to the 2.249-Mev level of Ca^{45}.

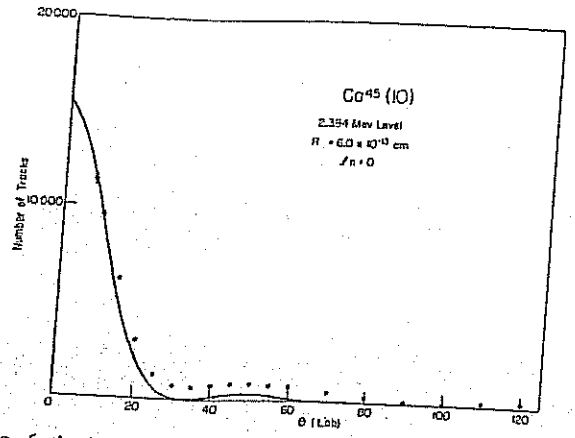

FIG. 6. Angular distribution of the proton group corresponding to the 2.394-Mev level of Ca^{45}.

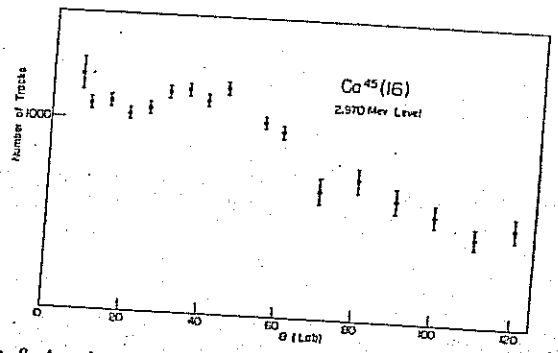

FIG. 8. Angular distribution of the proton group corresponding to the 2.970-Mev level of Ca^{45}.

angular distributions. The errors shown are standard statistical counting errors only. Because of the presence of carbon and oxygen in the target, some levels of Ca^{45} could not be observed at certain angles, since they were masked by intense proton groups from the $C^{12}(d,p)C^{13}$ and $O^{16}(d,p)O^{17}$ reactions. This situation is demonstrated in Fig. 1 at a plate distance of 36 cm.

The stripping curves shown in the results were constructed from the nomograms prepared by Lubitz and Parkinson.[9] The curves, as plotted, are not corrected for the difference between θ_{lab} and $\theta_{c.m.}$, or for the difference between the solid angle in the laboratory and in the center-of-mass coordinates. These corrections for the excited level at 3.419 Mev are:

$\theta_{c.m.}$	θ_{lab}	$\Delta\theta$	$d\Omega_{c.m.}/d\Omega_{lab}$
10°	9° 43′	17′	0.944
50°	48° 48′	1° 12′	0.967

The corrections for this state are largest, since it has the lowest Q value. Where the maxima occur, both corrections are smaller than the error introduced by the nomograms from which the stripping curves were calculated.

The interaction radius, R, is an adjustable parameter in the calculation of the theoretical angular distributions. Huby[10] has stated that the formula $R=(1.22A^{\frac{1}{3}}+1.7)\times10^{-13}$ cm gives a radius that will normally support unique determinations of l_n. This formula gives $R=6.0\times10^{-13}$ cm for Ca^{45}. The results of the present experiment, together with angular distributions for (d,p) reactions on other calcium isotopes,[8,11] indicate that no single value of R will lead to unambiguous values of l_n for all the calcium levels investigated. However, 6.0×10^{-13} cm appears to be a reasonable compromise; this value was used in the calculations of the graphs displayed in Figs. 2 through 11. Further discussion of the difficulties in assigning R may be found in reference 8.

Table I lists the values of the orbital angular momentum quantum number that gives the best fit to the data, using $R=6.0\times10^{-13}$ cm. The intensity of the peaks from the various levels at their angle of maximum

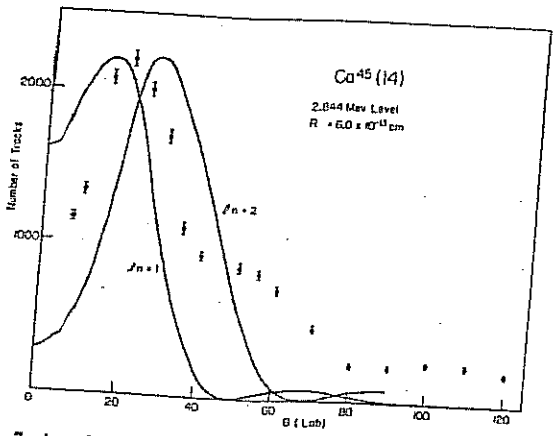

FIG. 7. Angular distribution of the proton group corresponding to the 2.844-Mev level of Ca^{45}.

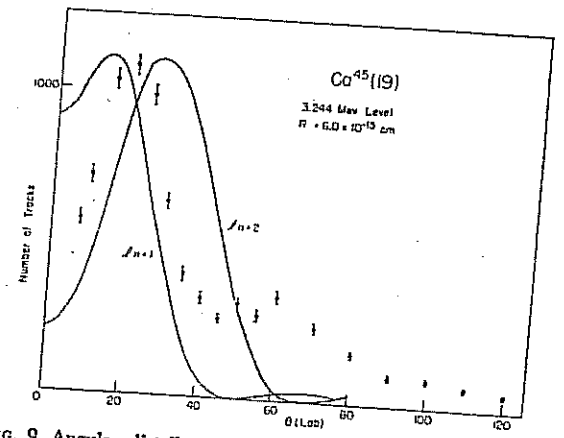

FIG. 9. Angular distribution of the proton group corresponding to the 3.244-Mev level of Ca^{45}.

[9] C. R. Lubitz and W. C. Parkinson, Rev. Sci. Instr. 26, 400 (1955).

[10] R. Huby, *Progress in Nuclear Physics*, edited by O. R. Frisch (Pergamon Press, London, 1953), Vol. 3.

[11] C. K. Bockelman, Bull. Am. Phys. Soc. Ser. II, 1, 223 (1956).

yield was compared with the intensity of the ground state at $\theta=40$ degrees in order to calculate the relative differential cross sections. These relative cross sections and the angle at which they were compared are listed in Table I. In these calculations, solid-angle corrections[7]

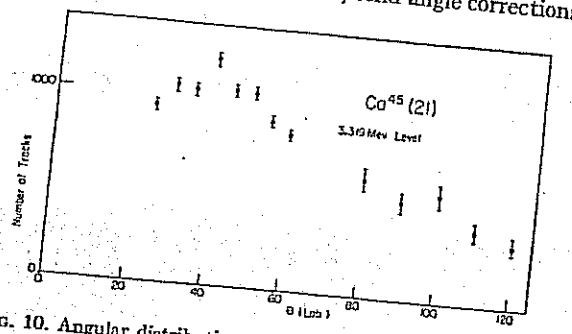

FIG. 10. Angular distribution of the proton group corresponding to the 3.319-Mev level of Ca^{45}.

were used to account for the different locations on the focal surface of the proton groups. The excitation energies given in Table I are taken from Braams's experiment.[1] Also listed are levels observed by Braams which were not seen in sufficient intensity to measure an angular distribution. The upper limit on intensity for these groups was derived from the 3000-microcoulomb exposures at 20 and 50 degrees.

Although the target contained only 1.87% Ca^{40}, the group corresponding to the first excited state in Ca^{41} was

TABLE I. Relative intensities of proton groups associated with levels in Ca^{45}.

Level	Excitation	Angle of maximum yield	Relative yield at maximum	l_n
0	0	40°	1.00	
1	0.176	50	0.030	3
2	(1.036)		<0.11	...
3	1.432	20	2.00	
4	(1.475)		<0.07	1
5	(1.557)		<0.06	
6	1.902	20	11.5	
7	1.971	50	0.031	1
8	2.249	15	1.90	...
9	2.356	30	0.017	1
10	2.394	<7½	1.90(7½°)	...
11	(2.597)		<0.04	0
12	2.681	20	0.039	
13	(2.763)		<0.08	...
14	2.844	20	2.12	
15	2.950		<0.05	1 or 2
16	2.970	10	0.195	
17	(3.032)		<0.10	...
18	3.148		<0.05	
19	3.244	20	1.04	
20	3.296		<0.04	1 or 2
21	3.319	40	0.189	
22	3.419	15	4.30	...
				1 or 2

sufficiently intense at the forward angles to obtain the cross section for the formation of this state at its angle of maximum yield (20 degrees) relative to the cross section for the formation of the Ca^{45} ground state at its angle of maximum yield (40 degrees). The ratio obtained is 14.2 ± 0.8, assuming the isotopic abundances given by Oak Ridge for the sample used are correct.

In conclusion, agreement with the stripping theory seems adequate to assign values of l_n with assurance from the distributions for the first five entries in

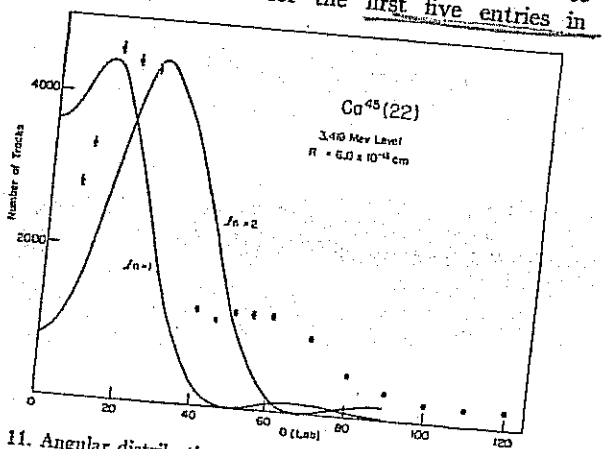

FIG. 11. Angular distribution of the proton group corresponding to the 3.419-Mev level of Ca^{45}.

column 5, Table I. The next three assignments of l_n are ambiguous. No attempt has been made to include in the stripping curves any effect of Coulomb forces. Since the results of Tobocman and Kalos[12] indicate that this effect tends to displace the maxima of the curves to higher angles, some preference is expressed here for the choice of the smaller of the two values of l_n.

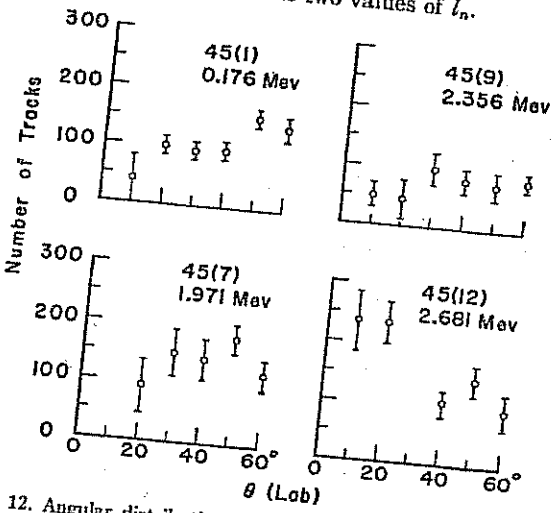

FIG. 12. Angular distributions of the four least intense proton groups corresponding to individual levels in Ca^{45}.

ACKNOWLEDGMENTS

The authors wish to express their appreciation to Dr. Charles K. Bockelman for his guidance during the course of this work and to the other members of the staff of the High Voltage Laboratory for their assistance in many ways.

[12] W. Tobocman and M. H. Kalos, Phys. Rev. 97, 132 (1955).